REPORT DOCUMENTATION PAGE

Form Approved
OMB No. 0704-0188

1. REPORT DATE *(DD-MM-YYYY)*
30-Sep-2008

2. REPORT TYPE
REPRINT

3. DATES COVERED *(From - To)*

4. TITLE AND SUBTITLE
A NEW REGIONAL 3-D VELOCITY MODEL FOR ASIA FROM THE JOINT INVERSION OF P-WAVE TRAVEL TIMES AND SURFACE-WAVE DISPERSION DATA

5a. CONTRACT NUMBER
FA8718-04-C-0027

5b. GRANT NUMBER

5c. PROGRAM ELEMENT NUMBER
62601F

6. AUTHOR(S)
Delaine T. Reiter[1] and William L. Rodi[2]

5d. PROJECT NUMBER
1010

5e. TASK NUMBER
SM

5f. WORK UNIT NUMBER
A1

7. PERFORMING ORGANIZATION NAME(S) AND ADDRESS(ES)
Weston Geophysical Corporation
181 Bedford St., Suite 1
Lexington, MA 02420

8. PERFORMING ORGANIZATION REPORT NUMBER

9. SPONSORING / MONITORING AGENCY NAME(S) AND ADDRESS(ES)
Air Force Research Laboratory
29 Randolph Road
Hanscom AFB, MA 01731-3010

10. SPONSOR/MONITOR'S ACRONYM(S)
AFRL/RVBYE

11. SPONSOR/MONITOR'S REPORT NUMBER(S)
AFRL-RV-HA-TR-2008-1075

12. DISTRIBUTION / AVAILABILITY STATEMENT
Approved for Public Release; Distribution Unlimited.

Weston Geophysical Corp.[1] and Massachusetts Institute of Technology[2]

13. SUPPLEMENTARY NOTES
Reprinted from: Proceedings of the 30th Monitoring Research Review – Ground-Based Nuclear Explosion Monitoring Technologies, 23 – 25 September 2008, Portsmouth, VA, Volume I pp 213 - 221.

14. ABSTRACT Accurate travel-time predictions for regional seismic phases are essential for locating small seismic events with the accuracy needed for nuclear monitoring decisions. Travel times calculated through a three-dimensional (3-D) Earth model have the best chance of achieving acceptable prediction errors, if the model is constrained by sufficient data. With this motivation, we have developed a self-consistent 3-D *P* and *S* velocity model of the crust and upper mantle in a large region of southern and central Asia to a depth of approximately 400 km. Our new model is the result of a nonlinear, joint body-wave/surface-wave inversion method applied to *Pn* travel times collected from the Engdahl, van der Hilst, and Buland (EHB) bulletin and group-velocity measurements provided by the University of Colorado and Lawrence Livermore National Laboratory. Consistency between the *P* and *S* velocities is achieved by imposing bounds on Poisson's ratio and by invoking a regularization constraint that correlates variations in *P* and *S* velocity from an initial model. We have tested our new model for its predictive capabilities using data from a large database of ground-truth events, which were held out from the joint inversion. The tests include the relocation of the ground-truth events, using data sets of *Pn*-only and *Pn*/*Sn* arrivals, and the direct comparison of predicted *Pn* and *Sn* travel times to the ground-truth observations. Both types of tests indicate that our 3-D inversion model has much better predictive capability than either a 1-D global model or our initial model, which comprised a 3-D crustal structure overlying a 1-D mantle. Importantly, our *S* velocity model performed well in predicting *Sn* times, even though such data were not included in our joint inversion. This achievement relied on the use of anelastic corrections in surface-wave modeling, however, which raises the stakes on deriving good Q models for complex regions like southern Asia. A final task in our project is to calculate the uncertainty of the new velocity model. We have begun to address this challenging task by developing numerical algorithms to compute two types of uncertainty measures. The first measure comprises slices of the posterior velocity covariance function for selected points in the inversion model. The second uncertainty measure translates model uncertainty to travel-time prediction uncertainty in the form of the posterior variance/covariance matrix of the travel-time prediction errors along a set of paths, such as those between a fixed event location to a network of regional stations.

15. SUBJECT TERMS
Seismic attenuation, Seismic propagation, Seismic characterization

16. SECURITY CLASSIFICATION OF:			17. LIMITATION OF ABSTRACT	18. NUMBER OF PAGES	19a. NAME OF RESPONSIBLE PERSON
a. REPORT	b. ABSTRACT	c. THIS PAGE			Robert J. Raistrick
UNCLAS	UNCLAS	UNCLAS	SAR	9	19b. TELEPHONE NUMBER *(include area code)* 781-377-3726

A NEW REGIONAL 3-D VELOCITY MODEL FOR ASIA FROM THE JOINT INVERSION OF P-WAVE TRAVEL TIMES AND SURFACE-WAVE DISPERSION DATA

Delaine T. Reiter[1] and William L. Rodi[2]

Weston Geophysical Corp.[1] and Massachusetts Institute of Technology[2]

Sponsored by Air Force Research Laboratory

Contract No. FA8718-04-C-0027
Proposal No. BAA04-67

ABSTRACT

Accurate travel-time predictions for regional seismic phases are essential for locating small seismic events with the accuracy needed for nuclear monitoring decisions. Travel times calculated through a three-dimensional (3-D) Earth model have the best chance of achieving acceptable prediction errors, if the model is constrained by sufficient data. With this motivation, we have developed a self-consistent 3-D *P* and *S* velocity model of the crust and upper mantle in a large region of southern and central Asia to a depth of approximately 400 km. Our new model is the result of a nonlinear, joint body-wave/surface-wave inversion method applied to *Pn* travel times collected from the Engdahl, van der Hilst, and Buland (EHB) bulletin and group-velocity measurements provided by the University of Colorado and Lawrence Livermore National Laboratory. Consistency between the *P* and *S* velocities is achieved by imposing bounds on Poisson's ratio and by invoking a regularization constraint that correlates variations in *P* and *S* velocity from an initial model.

We have tested our new model for its predictive capabilities using data from a large database of ground-truth events, which were held out from the joint inversion. The tests include the relocation of the ground-truth events, using data sets of *Pn*-only and *Pn*/*Sn* arrivals, and the direct comparison of predicted *Pn* and *Sn* travel times to the ground-truth observations. Both types of tests indicate that our 3-D inversion model has much better predictive capability than either a 1-D global model or our initial model, which comprised a 3-D crustal structure overlying a 1-D mantle. Importantly, our *S* velocity model performed well in predicting *Sn* times, even though such data were not included in our joint inversion. This achievement relied on the use of anelastic corrections in surface-wave modeling, however, which raises the stakes on deriving good Q models for complex regions like southern Asia.

A final task in our project is to calculate the uncertainty of the new velocity model. We have begun to address this challenging task by developing numerical algorithms to compute two types of uncertainty measures. The first measure comprises slices of the posterior velocity covariance function for selected points in the inversion model. The second uncertainty measure translates model uncertainty to travel-time prediction uncertainty in the form of the posterior variance/covariance matrix of the travel-time prediction errors along a set of paths, such as those between a fixed event location to a network of regional stations.

OBJECTIVES

The development and validation of accurate 3-D velocity models of the crust and upper mantle for regions of nuclear monitoring interest remains an important goal for nuclear monitoring organizations. Systematic biases caused by inadequately modeled Earth structures cause errors in the estimation of geophysical parameters such as the travel times and amplitudes of regional seismic phases. More accurate and reliable estimates of these quantities (especially in aseismic regions) will improve nuclear monitoring efforts to detect, locate, and discriminate regional events.

We have developed a joint 3-D inversion technique that incorporates both compressional-wave travel times and Rayleigh-wave group velocity measurements to determine the full *P* and *S* velocity structure of the crust and upper mantle. We have applied our algorithm to data from the broad region shown in Figure 1 to develop a new model, which we call *JWM* (for ***J***oint ***W***eston/***M***IT). In this paper we report on our efforts to validate the *JWM* model, as well as characterize its uncertainty using two new numerical approaches.

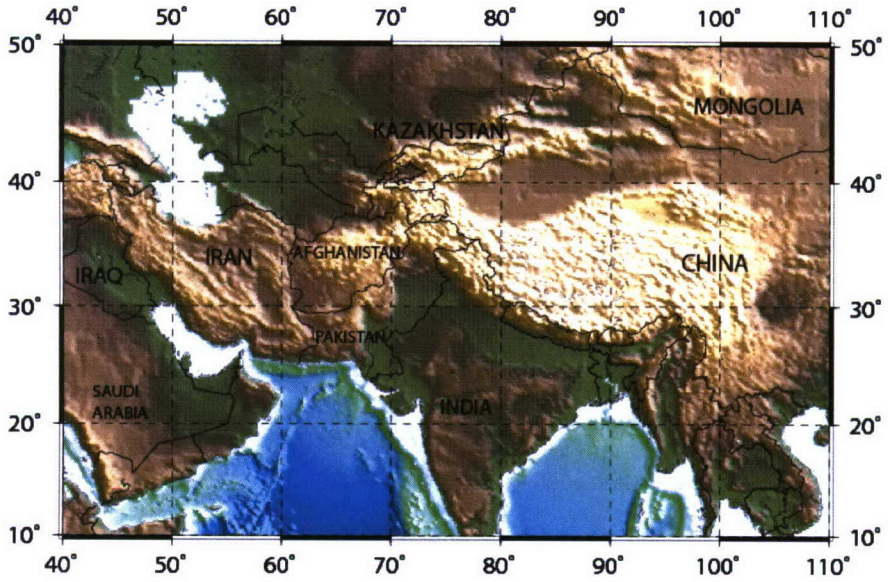

Figure 1. Topographic map of study region, which encompasses most of central and southern Asia, as well as the eastern side of the Middle East.

RESEARCH ACCOMPLISHED

In Rodi and Reiter (2007) we provide a summary of the methodologies and data sets used in our joint inversion, and we refer the reader to that paper for more details on the development of the inversion model. During the past year we have incorporated a number of subtle, but important, changes to the inversion algorithm, data sets, and model parameterization and constraints. For example, we now incorporate anelastic corrections in our surface-wave dispersion modeling to help address discrepancies between the shear-wave models found using surface-wave measurements versus those from body-wave measurements. We compute these corrections using the relationships developed by Liu et al. (1976) and Yu and Mitchell (1979) and an attenuation profile (Qp and Qs) associated with the AK135 global reference model (Montagner and Kennett, 1996; Kennett et al., 1995). The attenuation profile is held constant everywhere in our model, except over the Tibetan Plateau, where we halve the crustal and uppermost mantle Q values to better agree with studies that indicate high attenuation in the crust for paths traversing the Plateau (e.g., Rodgers and Schwartz, 1998).

We have also expanded the travel time database used in the *P*-wave tomography. Our predominant source of arrival-time observations is the EHB bulletin from the years 1982–2004 (Engdahl et al., 1998). We have augmented the EHB bulletin picks over the Tibetan Plateau and southwestern China using data from temporary arrays, courtesy of Dr. Chang Li (pers. comm.; Li et al., 2006). As in Rodi and Reiter (2007) we compressed this data set by forming

summary events on a regular grid having 0.5-degree spacing in latitude and longitude and containing 13 nodes in depth between 0 and 200 km, with the depth spacing per node increasing from 5 to 20 km. The final database used in the body-wave tomography contains 104,065 arrivals for 3,689 summary events and 603 stations.

Another change we have implemented involves a slight modification of our 3-D model parameterization in the upper mantle. Previously we represented the upper mantle model from the bottom of the crust to the discontinuity at a 410-km depth with nine nodes in the vertical direction. We have doubled that sampling with the use of 17 vertical nodes in order to better represent any velocity gradients present in this depth interval.

Finally, we have adjusted the prior error levels and correlation lengths used in our geostatistical regularization.

Joint Inversion Results

In Figure 2, we show two vertical, or depth, slices through the most current version of the *JWM* model along great-circle paths. On the left is a slice across the Saudi Arabian Peninsula to the northeast across southern Iran and into eastern Kazakhstan. One feature in this slice is the high velocity area with respect to the background model beneath the Makran orogeny in southern Iran. The V_P model shows these subsurface features most clearly, while the V_S model only hints at it. There is also an interesting low velocity feature in both the V_P and V_S models beneath central Iran, which may have interesting implications for the active subduction processes occurring beneath the Eurasian continental collision zone. The slice on the right cuts across the Himalayan Front, stretching from northern India into central China. Here the *Vp* and *Vs* models are somewhat anti-correlated across the southernmost portion of the Tibetan Plateau, with a stronger low in *Vs* than in *Vp*. We find that the Poisson's ratio across the Plateau is strongly elevated, which agrees with some previous studies in the region (e.g., Owens and Zandt, 1997). However, in contrast with some travel-time based studies, we find fairly strong velocity lows in the uppermost mantle in the northern portion of the Tibetan Plateau.

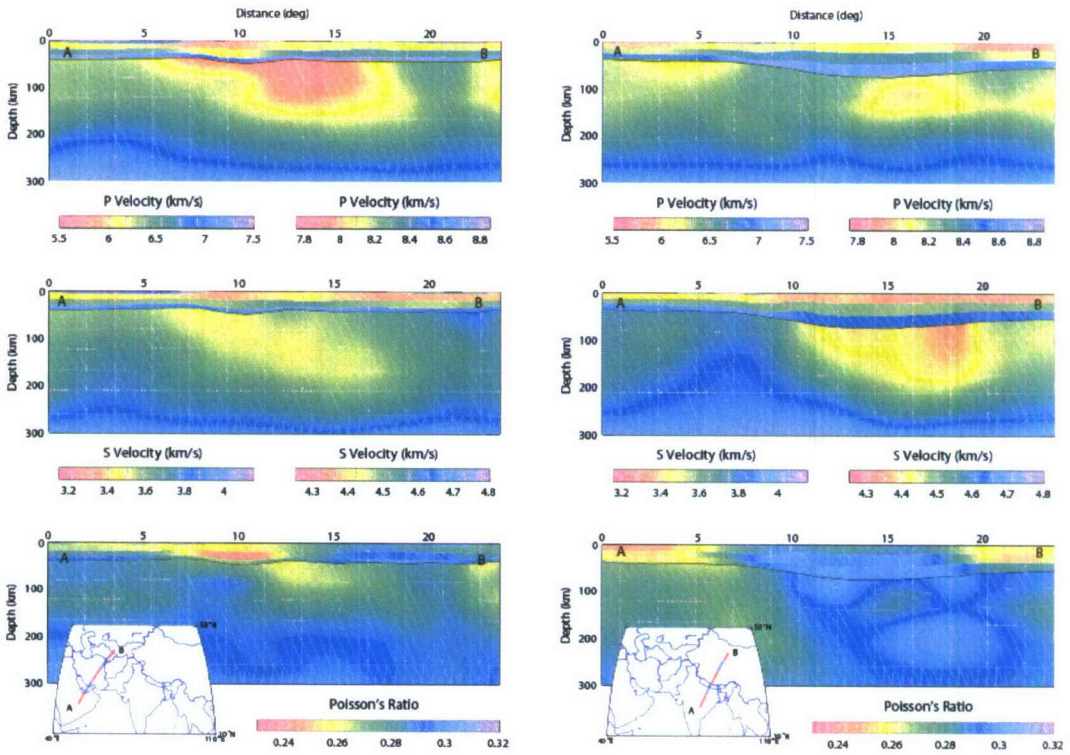

Figure 2. Depth slices along two great-circle paths (see inset maps for path AB) in the *JWM* inversion model, including V_P (top), V_S (middle), and Poisson's ratio (bottom). Note that a different color scale is used for crust and upper mantle velocities.

Validation Exercises

We have employed two validation techniques to assess the performance of the *JWM* crust/upper mantle velocity model. First, we have assessed the ability of *JWM* to predict regional travel-time observations for a set of ground-truth (GT) events. Our GT database of explosions and shallow earthquakes was derived from several sources, including the EHB bulletin, the Group2 Reference Event List (REL; Bondár et al., 2004a) and a list developed by Dr. Bob Engdahl for an International Association of Seismology and Physics of the Earth's Interior (IASPEI) location workshop (Engdahl, 2006). In Figure 3a we show the events in our GT database that are within the resolved boundaries of the *JWM* model (10–50°N, 40–110°E). The GT database contains high-quality epicenters, but the Group2 events do not include a large number of regional *P* and *S* observations. Therefore, we cross-referenced the Group2 REL events to the EHB bulletin (Engdahl et al., 1998) to retrieve a larger set of regional observations. This filtering exercise produced a validation dataset of 180 explosions and 225 earthquakes, with 2,990 *Pg*, *Pb*, or *Pn* first arrivals and 1,796 *Sg*, *Sb*, or *Sn* arrivals. The great-circle paths of the *P* and *S* GT observations are shown in Figure 3b and 3c, respectively. It is notable that the region of the inversion model that is sampled by the GT data raypaths is quite limited, which illustrates the difficulty of validating a model in this manner.

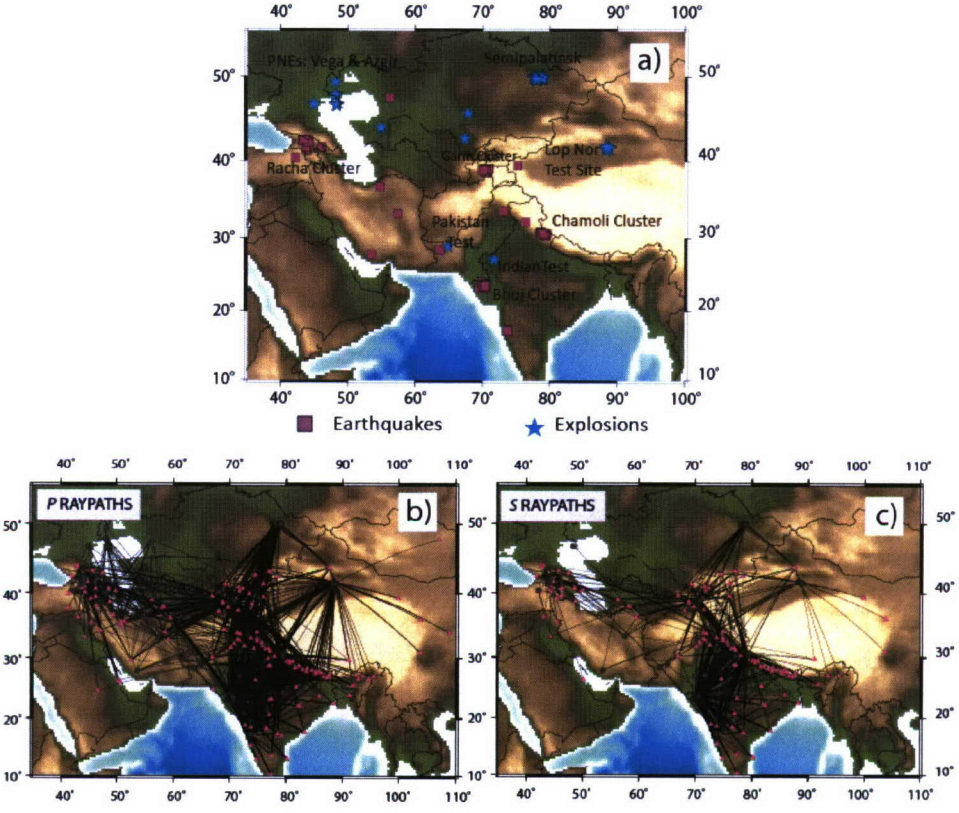

Figure 3. Ground-truth epicenters (GT0-GT7) in the resolved regions of the *JWM* model. (a) explosions (blue stars) and earthquakes (purple squares) within our region; (b) great-circle raypaths for the EHB *P* observations associated with events in the GT dataset; and (c) great-circle *S* raypaths.

We then predict the travel times of our regional GT observations through *JWM* using a 3-D finite-difference technique (Podvin and LeComte, 1991) and determine residuals with respect to the GT observed data. In Figure 4 we show the results of this exercise. To make it easier to see the trends in the data, we bin and average the residuals as a function of station-to-event epicentral distance. Figure 4 compares the residuals of the GT data relative to the AK135 reference model and to the 3-D *JWM* model. This validation, or 'prediction capability' test, demonstrates that we met the objectives of our study for the *P* travel times, but the *S* fits for JWM are not as good as we hoped they would be. One likely cause of the degraded fit of our model to the GT *S* data is the well-known '*S* discrepancy' between surface waves and body waves that other researchers have described (Baig and Dahlen, 2004; Montagner

and Kennett, 1996; Nolet and Moser, 1993). We note that the inclusion of anelastic corrections in the surface wave modeling has improved the *S* fits over previous versions of our inversion model. However, the corrections are just not quite enough to completely eliminate the negative bias that indicates our *S* model is perhaps 1%–2% too slow along the raypaths sampled by the GT *S*-wave data.

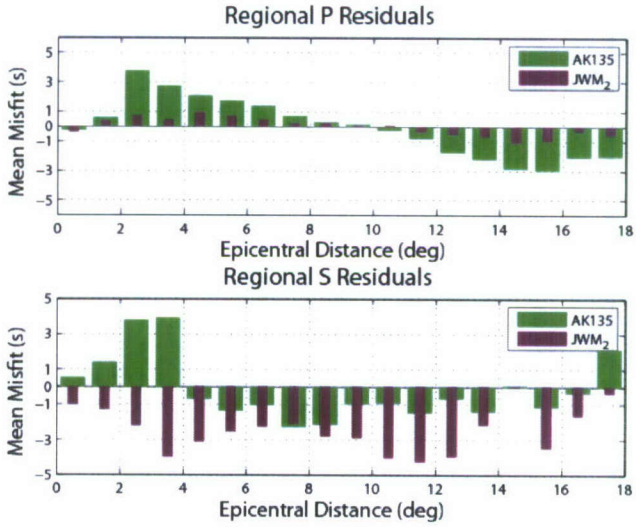

Figure 4. Mean GT travel-time residual binned as a function of epicentral distance for the AK135 model (green bars) and the *JWM* model (purple bars). Top subplots show the *P* residuals, and bottom subplots show the *S* residuals (1,796 arrivals).

In a second validation test we relocated a subset of events in our GT database to test the epicentral location accuracy of the *JWM* model. To avoid the most deleterious effects of poor network geometry on the solutions, we filtered the GT data to include only those events whose regional station distribution within our model has a secondary azimuthal gap less than 180°. Secondary azimuth gap (the largest azimuth gap when a single station of the network is removed) is a good proxy for the quality of the network coverage (Bondár et al., 2004b). This filtering reduced the testing data set to a list of 18 explosions and 54 earthquakes within our region, with 1,738 regional *P*-wave arrivals and 530 regional *S*–wave arrivals. The left side of Figure 5 shows the locations of our relocation events, color-coded according to the secondary azimuth gap of the regional arrivals.

We used the Grid-search Multiple-Event Location (GMEL) algorithm (Rodi, 2006) to relocate the events shown in Figure 5, first by including the regional *P* arrivals that fall within the confines of the model. Our GT relocation experiments were done with event depths fixed to their reported values. The subplot on the top right in Figure 5 compares the epicenter mislocations resulting with AK135 versus *JWM* travel-time predictions. Events that fall above the black unity line indicate 'wins' for the *JWM* model. The results show that *JWM* performs better than AK135 for all of the explosions and most of the earthquakes. On the bottom right of Figure 5 we show the comparison between AK135 and *JWM* for the case when both regional *P* and *S* arrivals are included. These results do not indicate a clear win for *JWM* over AK135 when the *S*-wave times are used to relocate the events. This is consistent with the decreased fits of the S model to the GT data, which reduces the effectiveness of the 3-D model to relocate better than the 1-D model. We note that a more detailed analysis of the individual events will likely yield more information about the relative performance of the 1-D and 3-D models in different sub-regions of our study area and how the performance might depend on network geometry.

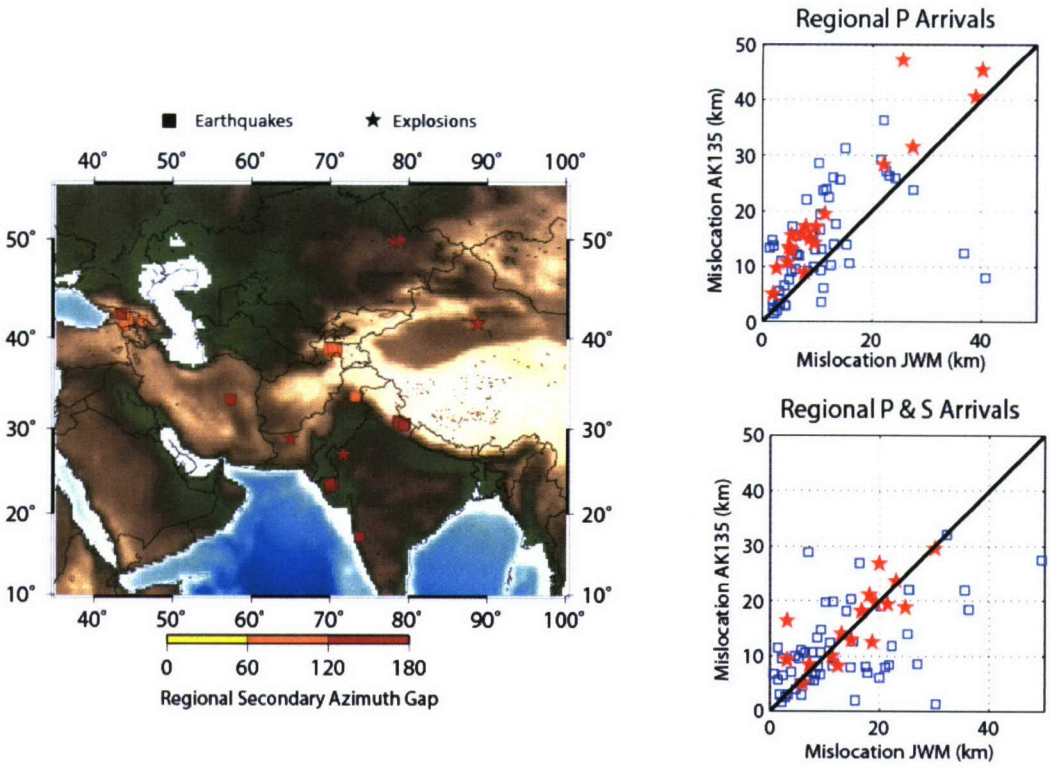

Figure 5. Results from epicentral mislocation tests. Left: Map of events (54 earthquakes, 18 explosions) from our GT database that meet regional network criteria for the relocation exercise; they are color-coded by their regional secondary azimuth gap. Right: Epicenter mislocations for *AK135* versus *JWM* when either regional P arrivals (top) or regional P and S arrivals are used in the relocations. Events that fall above the black unity line indicate 'wins' for the *JWM* model.

Calculation of Model Uncertainty

Our joint inversion method is consistent with a Bayesian approach to model uncertainty, in that the regularization used in both the body-wave and surface-wave inversion steps can be related to a prior mean and covariance on the unknown velocity model. The prior mean is our initial background model, comprising a 3-D crustal structure over the 1-D AK135 mantle, while the prior covariance is given in terms of a geostatistical characterization of the error in the background model, parameterized by the variance and vertical and horizontal correlation lengths of velocity heterogeneity relative to the background. Formally, Bayesian inference defines a posterior probability distribution on the velocity model, which implies a posterior mean and covariance, and other statistical properties, of the velocity model. In a linear inverse problem, the poster mean is taken as the optimal Bayesian estimate of the true Earth model and the posterior covariance describes the uncertainty in that estimate. In a nonlinear inverse problem, like the body-wave and surface-wave problems we address, it becomes somewhat more problematical to define, and compute, an optimal estimate and its uncertainty.

We are implementing the Bayesian framework for model uncertainty under some approximations and restrictions. We adopt a standard approach to nonlinear geophysical inversion (see, for example, Tarantola, 1987) and take the optimal model estimate to be the "maximum a posteriori" (MAP) model, which minimizes the regularized objective function for the problem and, accordingly, maximizes the posterior probability density function of the model. We characterize the uncertainty in the MAP estimate with the posterior covariance, evaluated under a linear approximation to forward problem. The most significant approximation we are making, however, is a practical consequence of our separating the joint body-wave/surface-wave problem into alternating steps of body-wave and surface-wave inversion. That is, we evaluate model uncertainty in the separated problems, ignoring the model constraints we have imposed to couple them.

Under these restrictions, we are developing numerical algorithms to compute two types of uncertainty measures, each of which can be used for either prior or posterior uncertainty. The first algorithm computes 'slices' of the the operator that defines the covariance between the velocity at two arbitrary points. A slice of the operator yields the variance of the velocity at a fixed reference point and its correlation with other points. Figure 6 shows examples of these model covariance slices, computed for the JWM P-wave velocity inversion model. On the left side of Figure 6 we show prior (top) and posterior (bottom) covariance slices for a shallow reference point near the center of our study region (30°N, 75°E, 60 km depth). Note the de-correlation between the crust and upper mantle in the prior covariance image, which is an intentional constraint in our regularization. The posterior covariance incorporates the travel-time data, which consequently reduces the posterior covariance. The right side of Figure 6 corresponds to a different reference point near the southwest corner of our study region (15°N, 45°E, 120 km depth). The prior and posterior covariance plots are similar to each other in this case because there is a dearth of travel-time data to constrain the model at this point.

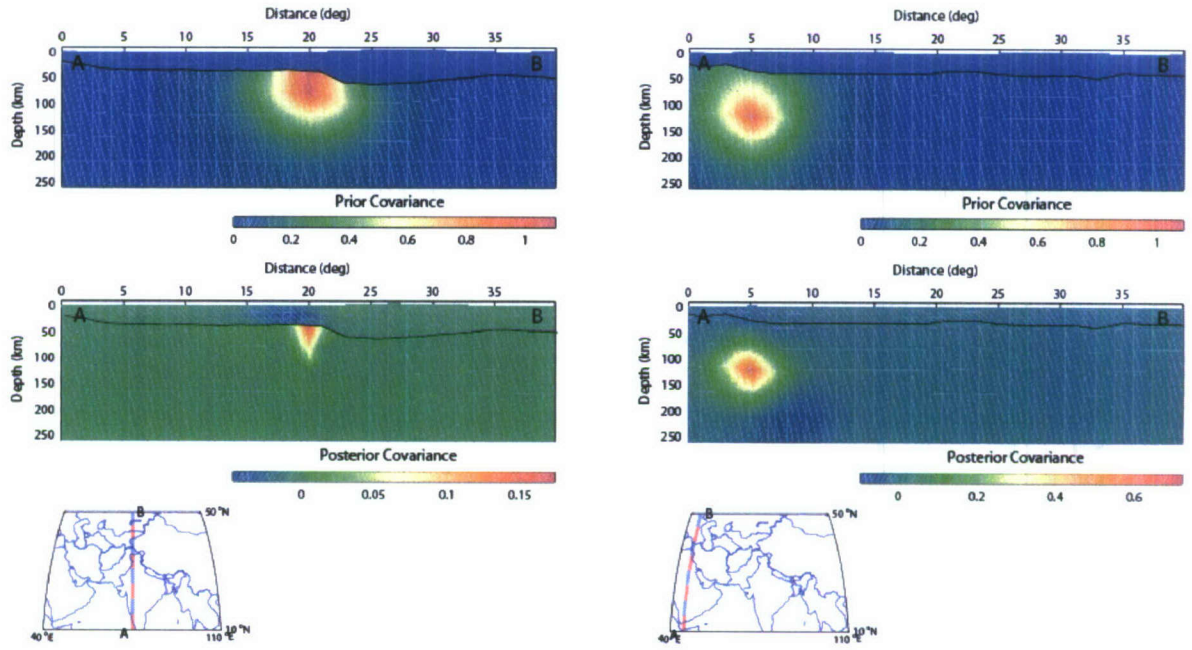

Figure 6. Vertical cross-sections through prior (top) and posterior (middle) covariance slices for the JWM P-wave model. Slices are shown for a reference point in the middle of the study region (left) and a reference point near the southwest corner of the study region (right). The section passes through their respective reference points and project as the AB lines in the bottom maps. The units of covariance are squared per cent.

The second uncertainty measure we compute is the variance/covariance matrix for the travel-time prediction errors along a set of paths; for example, from a fixed event location to a network of stations. This calculation allows us to translate the velocity uncertainty to travel-time prediction uncertainty. The algorithm for performing this translation is based on one developed for prior covariance matrices by Rodi and Myers (2007). To demonstrate this new capability, we mapped the covariance operator for the JWM P velocity model to the covariance matrix of P-wave travel-time prediction errors for an event in Iran (35°N, 58°E, 15 km). Twelve regional stations distributed from 1.8° to 17.5° recorded the event, as shown in Figure 7a. Figure 7b shows the prior and posterior standard-deviations of the travel-time predictions as a function of event-to-station distance, derived from the diagonal elements of the 12 by 12 covariance matrix.

The results in Figures 6 and 7 were based on the prior geostatistical parameters that were assumed in our most recent inversion. In particular, we assumed a 1% velocity standard deviation in both the crust and upper mantle. Rodi and

Myers (these Proceedings), however, find that larger velocity heterogeneity is more consistent with observed travel-time variability in Eurasia, such as 3% in the crust and 2% in the upper mantle. Based on these parameters, one would scale up the prior velocity covariances in Figure 6 by a factor of four and the prior travel-time standard deviations in Figure 7 by a factor of at least two. The impact of larger prior variances on posterior variances in Figures 6 and 7 is difficult to gauge since the posteriors depend also on the observational error variances assumed in the inversion, which would have to be reassessed if the priors are changed, an exercise underway. In any case, the posterior model variances will likely increase and translate to travel-time prediction error standard deviations noticeably larger than the rather small values seen in Figure 7b.

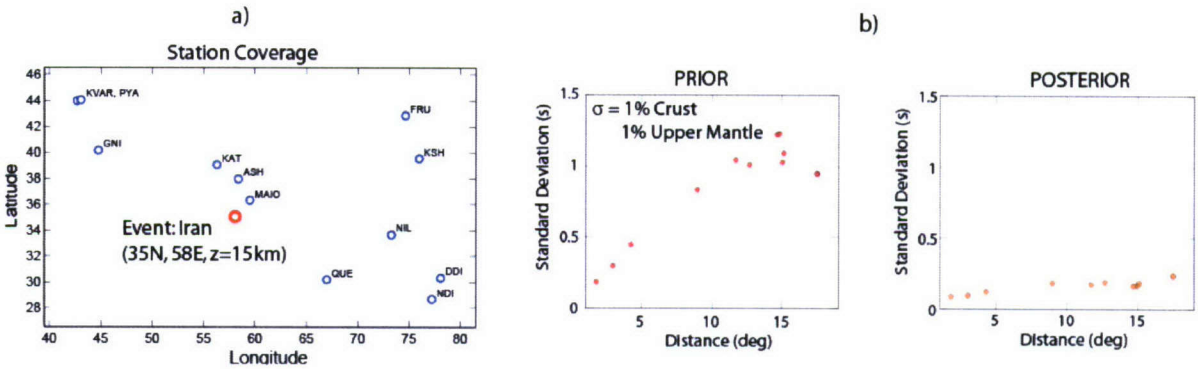

Figure 7. Example of travel-time prediction error calculations. a) Regional station distribution for an event in Iran; b) travel-time prediction-error standard deviations for 12 *Pn* paths, plotted as a function of distance. A prior standard deviation on the *P* velocity of 1% in the crust and upper mantle was assumed, leading to a unrealistically small travel-time standard deviation of less than 0.5 second.

CONCLUSIONS AND RECOMMENDATIONS

We have completed the development of a new V_P and V_S model for central and southern Asia using a new joint inversion technique that incorporates P-wave travel times and Rayleigh-wave group velocity data. The forward modeling incorporated in our inversion algorithm utilizes fully 3-D ray tracing for the body-wave travel times, and a two-step procedure for the surface-wave dispersion data that includes 1-D dispersion modeling at a geographic point followed by 2-D ray tracing in the phase velocity maps. We numerically solve the inverse problem using a set of iterated inversion steps, applying a set of geostatistically based model constraints.

In location validation exercises the model has proved to be very successful at both predicting travel times and locating GT events with regional observations. The prediction of observed GT *S* travel times continues to be less than satisfactory for some paths such as those across the Tibetan Plateau, although it has been improved by including anelastic corrections in our surface-wave modeling.

We have begun to analyze the uncertainty of our inversion model in a Bayesian framework. The uncertainty analysis is restricted to the separate body-wave and surface-wave inverse problems and ignores the model constraints we have imposed to couple them. We have developed algorithms to compute prior and posterior variances on the velocity model itself and on travel times predicted by the model. Our initial calculations indicate that travel-time prediction errors for Pn paths in the well-resolved portion of our model are 0.25 seconds or less, but this result depends on the rather small prior velocity standard deviation we assumed (1%), which we are considering increasing to a more realistic value.

REFERENCES

Baig, A. M. and F. A. Dahlen (2004). Traveltime biases in random media and the *S*-wave discrepancy, *Geophys. J. Int.* 158: 922–938.

Bondár, I., E. R. Engdahl, X. Yang, H. A. A. Ghalib, A. Hofstetter, V. Kirichenko, R. Wagner, I. Gupta, G. Ekström, E. Bergman, H. Israelsson, and K. McLaughlin (2004a). Collection of a reference event set for regional and teleseismic location calibration, *Bull. Seis. Soc. Am.* 94: 1528–1545.

Bondár, I., S. C. Myers, E. R. Engdahl, and E. A. Bergman (2004b). Epicentre accuracy based on seismic network criteria, *Geophys. J. Int.* 156: 483–496.

Engdahl, E.R. (2006). Application of an improved algorithm to high precision relocation of ISC test events, *Phys. Earth Planet. Interiors* 158: 14–18.

Engdahl E. R., R. van der Hilst, and R. Buland (1998). Global teleseismic earthquake relocation with improved travel times and procedures for depth determination, *Bull. Seis. Soc. Am.* 88: 722–743.

Kennett, B. L .N. Engdahl, E. R., and Buland R. (1995). Constraints on seismic velocities in the Earth from travel times, *Geophys. J. Int'l.* 122: 108–124.

Montagner, J.-P. and B. L. N. Kennett (1996). How to reconcile body-wave and normal-mode reference earth models, *Geophys. J. Int.* 125: 229–258.

Li, C., R. D. van der Hilst, and M. N. Toksöz (2006). Constraining *P* wave velocity variations in the upper mantle beneath Southeast Asia, *Phys. Earth Planet. Int.* 154: 180–195.

Liu, H.-P., D. L. Anderson, and H. Kanimori (1976). Velocity dispersion due to anelasticity; implications for seismology and mantle composition, *Geophys. J.R. Astr. Soc.* 47: 41–58.

Nolet, G., and T.-J. Moser (1993). Teleseismic delay times in a 3-D Earth and a new look at the *S* discrepancy, *Geophys. J. Int.*, 114, 185-195.

Owens, T. J. and G. Zandt (1997). Implications of crustal property variations for models of Tibetan plateau evolution. *Nature* 387: 37–43.

Podvin P., and I. Lecomte (1991). Finite difference computation of traveltimes in very contrasted velocity models: a massively parallel approach and its associated tools, *Geophys. J. Int.* 105: 271–284.

Rodi. W. (2006). Grid-search event location with non-Gaussian error models, *Phys. Earth. Planet. Int.* 158: 55–66.

Rodi, W. and D. T. Reiter (2007). *SAsia3D*: A 3-D crust and upper-mantle velocity model of South Asia derived from joint inversion of *P*-wave travel times and surface-wave dispersion data, in *Proceedings of the 29th Monitoring Research Review: Ground-Based Nuclear Explosion Monitoring*, LA-UR-07-5613, Vol. 1, pp. 236–245.

Rodi, W.L. and S. C. Myers (2007). Modeling travel-time correlations based on sensitivity kernels and correlated velocity anomalies, in *Proceedings of the 29th Monitoring Research Review*: *Ground-Based Nuclear Explosion Monitoring,* LA-UR-07-5613, Vol. 1, pp. 463–471.

Rodi, W. L. and S. C. Myers (2008). Modeling travel-time correlations based on sensitivity kernels and correlated velocity anomalies, these Proceedings.

Rodgers, A. J., and S. Y. Schwartz (1998). Lithospheric structure of the Qiangtang Terrane, northern Tibetan Plateau, from complete regional waveform modeling: Evidence for partial melt, *J. Geophys. Res.* 103: 7,137–7,152.

Tarantola, A. (1987). *Inverse Problem Theory*, Elsevier.

Yu, G.-Y., and B. J. Mitchell (1979). Regionalized shear velocity models of the Pacific upper mantle from observed Love and Rayleigh wave dispersion, *Geophys. J. R. Astr. Soc.* 57: 311–341.